

Optimizing Fiducial Marker Placement for Improved Visual Localization

Qiangqiang Huang¹, Joseph DeGol², Victor Fragoso², Sudipta N. Sinha², and John J. Leonard¹

Abstract—Adding fiducial markers to a scene is a well-known strategy for making visual localization algorithms more robust. Traditionally, these marker locations are selected by humans who are familiar with visual localization techniques. This paper explores the problem of automatic marker placement within a scene. Specifically, given a predetermined set of markers and a scene model, we compute optimized marker positions within the scene that can improve accuracy in visual localization. Our main contribution is a novel framework for modeling camera localizability that incorporates both natural scene features and artificial fiducial markers added to the scene. We present optimized marker placement (OMP), a greedy algorithm that is based on the camera localizability framework. We have also designed a simulation framework for testing marker placement algorithms on 3D models and images generated from synthetic scenes. We have evaluated OMP within this testbed and demonstrate an improvement in the localization rate by up to 20 percent on three different scenes.

I. INTRODUCTION

Visual localization is a foundational technique for applications including AR/VR, autonomous driving, and robotic navigation and manipulation. A typical problem in visual localization is to estimate the camera pose of a query image, provided a pre-built map. While the problem has long been investigated in many fields [1], visual localization still suffers due to challenging scenes such as textureless walls and repetitive structures (e.g., Rooms A and B in Fig. 1). One common solution to these challenges is to place fiducial markers as additional texture and identifiers in the scene [2], [3]; however, placing fiducial markers in larger environments is a time consuming process and the resulting performance improvement depends on marker positions. Thus, optimizing marker placement is valuable for robust visual localization.

This work proposes an automatic approach to optimizing marker placement such that 1) the resulting marker positions yield improved accuracy in visual localization and 2) a human user will be able to place markers at positions planned by the approach (e.g., no markers on the ceiling). Specifically, the approach computes optimized marker positions, given a predetermined set of markers and a scene model. The key contributions of this work include:

- 1) This is the first work that optimizes marker placement for visual localization based on scene features and fiducial markers.
- 2) We propose a novel framework that models localizability of camera poses in a scene and computes localizability

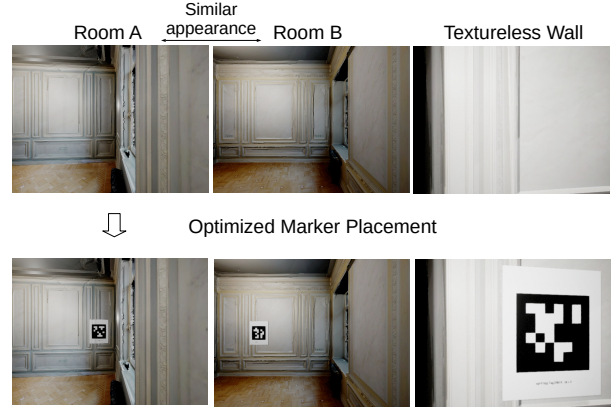


Fig. 1. Three challenging examples for visual localization within the same scene. The images on the left and middle show two almost identical rooms in the scene, whereas the image on the right depicts a very weakly textured surface. Marker placements¹ in this scene guided by our optimized marker placement approach led to improved visual localization on these examples.

scores.

- 3) We develop a greedy algorithm that optimizes marker positions with the goal of increased localizability scores.
- 4) We design a simulation framework for testing marker placement algorithms on 3D scene models that enables others to reproduce and build on our work.
- 5) We demonstrate that optimized marker placement by our approach can improve the localization rate by up to 20 percent on three different scenes.

Notation

Deterministic values are denoted by lowercase letters while random variables are indicated by uppercase letters. A set of values is denoted by calligraphic font (e.g., $\mathcal{L} = \{l\}$). We use $p(X)$ to denote the probability density function $p_X(\cdot)$ of random variable X .

II. RELATED WORK

We briefly review some recent work related to mapping and localization with fiducial markers and marker/landmark placement planning. Examples of fiducial markers include tag families with explicit IDs (e.g., ArUco markers [5], AprilTag [4], ChromaTag [6]) and emerging learning-based marker designs [7]. Fiducial markers are widely recognized as an effective approach for improving localization and mapping accuracy. DeGol et al. [3] demonstrate that marker IDs are useful in image matching and resectioning for structure from motion (SfM), leading to improvements in reconstruction

¹Computer Science and Artificial Intelligence Lab, Massachusetts Institute of Technology, Cambridge, MA 02139, USA {hqg, jleonard}@mit.edu

²Microsoft, Redmond, WA 98052, USA {jodegol, victor.fragoso, sudipta.sinha}@microsoft.com

¹Fiducial markers in the examples are AprilTags [4] but our algorithm is general and can be used with any existing family of fiducial markers.

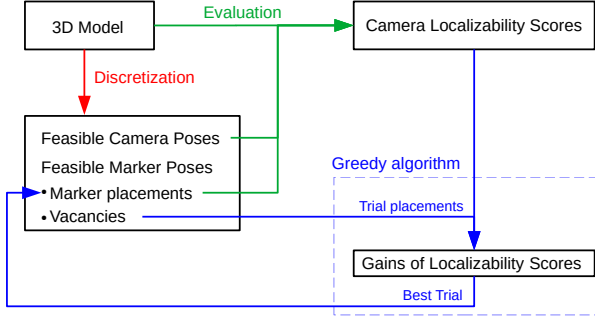


Fig. 2. An overview of our approach for optimizing marker placements. We first create a set of feasible camera poses and marker poses by discretizing space in the 3D model. Then we evaluate localizability scores of feasible camera poses in the 3D model and update the scores once a feasible marker pose is selected to place a marker. The marker placement is selected by a greedy algorithm as the best trial out of trial placements in the vacancies (unselected marker poses). These trial placements yield gains of localizability scores and are ranked by the gains.

results. The UcoSLAM system [2] integrates marker detection with a bag-of-words approach and presents more robust tracking and relocalization than SLAM techniques with no marker detection [8], [9]. However, marker placements in these SfM or SLAM systems are manually determined and not planned by algorithms.

To the best of our knowledge, there is no prior work on optimizing marker placement for visual localization based on scene features and fiducial markers. Existing related work focuses on landmark deployment for robotic localization without considering scene features [10]–[12]. Beinhofer et al. [13] explore optimal placement of artificial landmarks such that a robot equipped with range and/or bearing sensors repeatedly follows predetermined trajectories in planar environments with improved accuracy. Lei et al. [14] investigate landmark deployment for poses on $SE(3)$ and demonstrate placing fiducial markers in a cubic environment; however, features in the scene are not involved in optimizing the marker placement.

III. METHODS

We aim to compute k 3D locations in the scene for placing k fiducial markers such that after marker placement, the camera localization performance improves for query images from anywhere within the scene. We describe our optimized marker placement (OMP) approach in the following sections.

A. Assumptions

This work makes two assumptions:

- 1) A textured 3D model of the scene is available.
- 2) Markers and cameras are located on a 3D plane parallel to the ground plane at roughly the eye level of a person with average height.

Note that the textured model can be a 3D simulation environment or a dense reconstruction of scenes. We will collect images (e.g., RGB, depth, and surface normal) and corresponding camera poses from the model and take them as input to our approach for optimizing marker placement. The second assumption ensures that our marker placement will be reachable to a human user and constrains the number

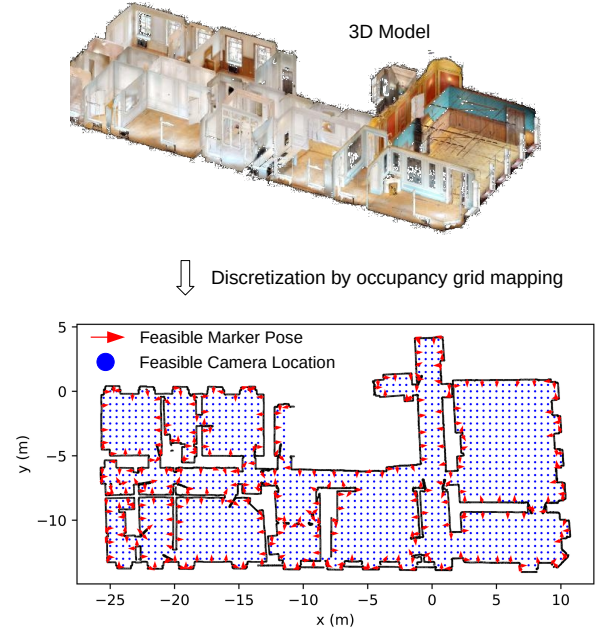


Fig. 3. Discretization of one of the 3D models from the Habitat-Matterport 3D dataset². We select a ground plane in the 3D model at roughly eye level of a human user and create an occupancy grid map of the plane using depth images. The discretized space of the ground plane consists of feasible marker poses (red arrows), which are sampled from scan points on the ground plane perimeter, and feasible camera locations (blue dots), which are centers of unoccupied cells.

of feasible camera and marker locations for the sake of computation efficiency.

B. Key Techniques

Fig. 2 shows an overview of our approach. The approach is composed of three key techniques: 1) discretization, 2) evaluation of camera localizability, and 3) a greedy algorithm for selecting marker placements.

1) *Discretization*: We first convert the ground plane in the 3D model to a discretized space of camera and marker poses, as shown in Fig. 3. The conversion is implemented by occupancy grid mapping. Specifically, given the 3D model, we synthesize pseudo laser scans in the ground plane and use them to create an occupancy grid. Centers of unoccupied grid cells are designated as feasible camera locations (dots in Fig. 3) while scan points form the perimeter of the free space (lines in Fig. 3). We uniformly downsample the scan points to generate a set of feasible marker poses \mathcal{M} on the perimeter of the ground plane (arrows in Fig. 3) whose orientations are determined by surface normals in the 3D model. We derive a set of feasible camera poses \mathcal{C} from the feasible camera locations. Each of the camera locations yields n camera poses whose optical axes are parallel to the ground plane and evenly spaced in $[0, 2\pi]$ (e.g., the default $n = 8$).

2) *Camera localizability score*: We compute camera localizability scores by evaluating uncertainty in localizing feasible camera poses. Specifically, for any feasible camera pose $c \in \mathcal{C}$ (the corresponding random variable is C), we synthesize

²The 3D model in the figure is provided by the Habitat-Matterport 3D Research Dataset (model name: 00770-NBg5UqG3di3) [15].

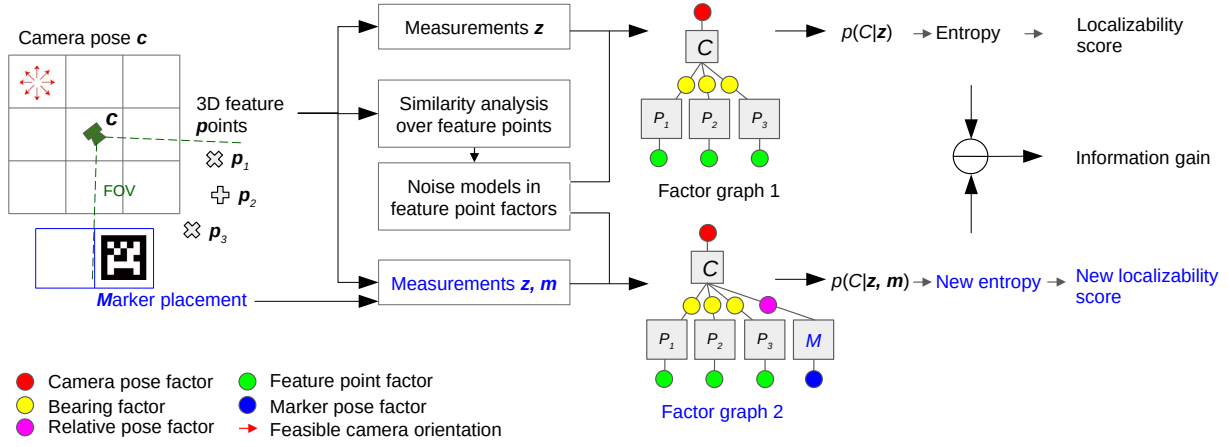


Fig. 4. Evaluation of localizability scores and the information gain brought by a marker placement. On the left we show a grid of feasible camera poses. Feasible camera poses are positioned at the center of cells with orientations shown as the red arrows. The field of view of camera pose c covers feature points p_1, p_2 , and p_3 in the 3D model and a marker placement on the discretized perimeter of the level set of the ground plane. We synthesize measurements z of feature points to create a camera localization problem using scene features. The problem is represented by factor graph 1 and distribution $p(C|z)$ by which we can compute entropy as well as localizability score of the camera pose seeing no markers. We penalize contributions of repetitive structures on the localizability score via the similarity analysis over scene features. With additional measurements m to the marker, we create another localization problem which is represented by factor graph 2 and distribution $p(C|z, m)$. The new problem leads to a new entropy and a new localizability score. The difference between old and new entropies defines the information gain at the camera pose yielded by the marker placement.

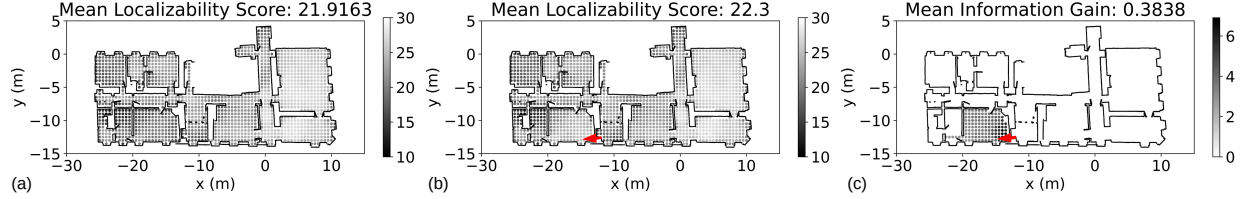


Fig. 5. Results of localizability scores: (a) no markers, (b) a trial marker placement (red arrow), and (c) the information gain. The score (or gain) at a dot is the mean score (or gain) of camera poses with all feasible orientations and the same location of the dot. The number of feasible orientations is 8. Darker dots stress low localizability scores in (a) and (b) and high information gains in (c).

measurements z to create a camera localization problem, estimate the distribution of the camera pose $p(C|z)$, and define the localizability score of the camera pose $l(c)$ as the negation of the entropy of the distribution, as shown in

$$l(c) = -H(p(C|z)) = \mathbb{E}[\ln p(C|z)]. \quad (1)$$

If a new fiducial marker is added in the field of view (FOV) of the camera pose, the new synthetic measurement regarding the marker will change the entropy of the camera pose distribution, resulting in an information gain that quantifies the impact of the marker placement. Fig. 4 summarizes steps for evaluating the localizability score and the information gain. These steps are explained in detail in following paragraphs.

Synthetic localization problems for computing the localizability score and information gain: The leftmost part of Fig. 4 illustrates feature points and a feasible marker pose (i.e., trial marker placement) that are in the FOV of a feasible camera pose. We collect RGB and depth images at the camera pose in the 3D model. These images will be used to compute 3D points and descriptors of features (e.g., SIFT [16]). We use these known poses and points to synthesize measurements and estimate probability density functions (PDFs) of the camera pose variable. The PDF enables computation of the entropy as well as the localizability score in (1). For example, measurements z in Fig. 4 contain the camera pose, the 3D

points of features, and bearings between the camera pose and the 3D points. Thus the PDF $p(C|z)$, which is represented by factor graph 1, expresses the distribution of the camera pose constrained by features. Placing a marker in the FOV of the camera leads to new synthetic measurements m of the marker pose and the relative pose between the marker and the camera. As a result, the camera pose is further constrained by measurements m thus is described by a new PDF $p(C|z, m)$ represented by factor graph 2 in Fig. 4. We use an approach that is similar to the one proposed by Stachniss et al. [17] to define the information gain of a marker placement. The information gain is defined as the change of entropy that the marker placement m yields at the camera pose c , as seen in

$$I(m, c) = H(p(C|z)) - H(p(C|z, m)). \quad (2)$$

Fig. 5a shows localizability scores of camera poses in the original ground plane with no marker placement. Note that the score at a dot in the figure is the mean score of camera poses with all feasible orientations. Fig. 5b shows localizability scores after adding a marker (the arrow) to the ground plane perimeter. The marker increases scores in the region around the marker, indicated by the brighter dots in the region in Fig. 5b and the information gain in Fig. 5c.

Similarity analysis over feature points: Repetitive structures in scenes cause similar features across RGB images and

Algorithm 1: Optimized Marker Placement (OMP)

Input: The number of markers k , the list of feasible marker poses \mathcal{M} , the ground plane space \mathcal{S}
Output: k marker poses
1 Initialize an empty list for storing selected marker poses \mathcal{O}
2 **repeat** k **times**
3 Initialize the best marker pose $T^* = \emptyset$
4 Initialize the highest localizability gain $g^* = -\inf$
5 Evaluate localizability scores \mathcal{L}^* of camera poses in space \mathcal{S}
6 **for** Pose T in \mathcal{M} **do**
7 Place a marker at pose T in space \mathcal{S}
8 Evaluate localizability scores \mathcal{L} of camera poses
9 Compute information gains $\mathcal{I} = \mathcal{L} - \mathcal{L}^*$
10 Evaluate localizability gain g of the marker by (6)
11 **if** $g > g^*$ **then**
12 $T^* = T$
13 $g^* = g$
14 Remove the marker from space \mathcal{S}
15 Push T^* to \mathcal{O}
16 Place a marker at pose T^* in space \mathcal{S}
17 Remove T^* from \mathcal{M}
18 **return** List of marker poses \mathcal{O}

can result in localizing to a wrong location. To reduce the contribution of repetitive structures to localizability scores, we penalize the localizability score of a camera pose if similar features appear in the FOV of the camera. Specifically, when modeling similar feature points in factor graphs, we set greater uncertainty in noise models of feature point factors to encode the fact that similar features are ambiguous and less informative. (3) shows the feature point factor that formulates the difference between noisy 3D location $\tilde{\mathbf{p}}$ and true 3D location \mathbf{p} using a Gaussian distribution

$$p(\tilde{\mathbf{p}}|\mathbf{p}) = \mathcal{N}(\tilde{\mathbf{p}} - \mathbf{p}; \mathbf{0}, \Sigma_{\mathbf{p}}) \quad (3)$$

where $\Sigma_{\mathbf{p}}$ is the covariance we set for modeling noise. For example, in the leftmost part of Fig. 4, feature points \mathbf{p}_1 and \mathbf{p}_3 are visually similar, so we set a big covariance in feature point factors of \mathbf{p}_1 and \mathbf{p}_3 . Informally speaking, factors with big covariances impose loose constraints on the camera pose distribution, leading to lower contributions on the localizability score. Thus the negative effect of repetitive structures is considered in the localizability score by modeling similar feature points in factor graphs with greater uncertainty.

We perform a similarity analysis over scene features to determine noise models in feature point factors (i.e., $\Sigma_{\mathbf{p}}$ in (3)), as shown in the flow chart in Fig. 4. The similarity analysis is to count the number of similar feature points to any feature point. The resulting covariance $\Sigma_{\mathbf{p}}$ for the query point \mathbf{p} is formulated as

$$\Sigma_{\mathbf{p}} = (1 + n_{\mathbf{p}})\Sigma_0 \quad (4)$$

where Σ_0 is a base covariance (e.g., $\text{diag}(2.5, 2.5, 2.5) \times 10^{-3} \text{ m}^2$ in our experiments) and $n_{\mathbf{p}}$ denotes the number of similar feature points to the query point \mathbf{p} . Feature points observed by all feasible camera poses are filtered to select similar feature points of a query feature point. The selection is determined by two criteria: 1) the selected feature points have similar descriptors to the query feature point and 2) 3D

locations of selected feature points are not too close to the 3D location of the query feature point. The intuition is that, if two areas in the scene look similar but they are far away from each other, a wrong place recognition would incur a huge localization error, so it is necessary to reflect such a situation in the localizability score.

Estimation of camera pose distributions: We use the Laplace approximation [18, Ch. 4.4] to estimate a Gaussian distribution that approximates the camera pose distribution encountered in the synthetic localization problem. The Gaussian distribution centers on the mode of the camera pose distribution which is simply the known feasible camera pose. The covariance Σ is the only unknown and can be approximated by an estimated Hessian of the negative logarithm of the camera pose distribution at the mode (see [19, Sec. 2] for the estimation of the covariance). Thus the entropy encountered in the synthetic localization problem can be approximated by the entropy of the Gaussian distribution, as seen in

$$H(p(C|\cdot)) \approx \frac{1}{2} \ln |\Sigma| + \frac{d}{2} (1 + \ln(2\pi)) \quad (5)$$

where the dimensionality d is 6 for 6DOF poses.

3) *The greedy algorithm:* The algorithm sequentially selects k poses from feasible marker poses \mathcal{M} (see Algorithm 1). The algorithm executes k loops to search the best k poses. In each loop, we update localizability scores, tentatively place a marker at any feasible marker pose, and compute localizability gains of trial marker placements. The best pose that earns the highest localizability gain will be removed from feasible marker poses and be permanently occupied by the marker. The new marker placement will influence the next update of localizability scores.

We summarize information gains for all feasible camera poses in the scene, using a single scalar quantity that we refer to as localizability gain. Informally, one could think of the localizability gain as the reward for placing an additional marker at a specific position. The localizability gain of any marker placement \mathbf{m} is defined as the q^{th} percentile of information gains at all feasible camera poses \mathcal{C} , as seen in

$$g(\mathbf{m}) = \inf\{i \in \mathbb{R} : F_I(i) \geq \frac{q}{100}\}, \quad (6)$$

where $F_I(\cdot)$ is the cumulative distribution function (CDF) of information gains

$$\mathcal{I} = \{I(\mathbf{m}, \mathbf{c}) : \mathbf{c} \in \mathcal{C}\}. \quad (7)$$

The choice of percentile $q \in [0, 100]$ is crucial and dependent on environments (i.e., the ground plane). For example, in a large environment where any marker is only visible to a small fraction of feasible camera poses, a low percentile q would likely incur zero localizability gain for all markers since the camera poses seeing no markers receive a zero information gain and constitute a great portion of the information gain distribution \mathcal{I} .

We use an adaptive approach to determine the percentile q before computing the localizability gain. The approach introduces a hyperparameter $v \in [0, 100]$ and ensures that the most visible v percent of markers earn nonzero localizability gains. A high v allows more markers, even the ones stuck in

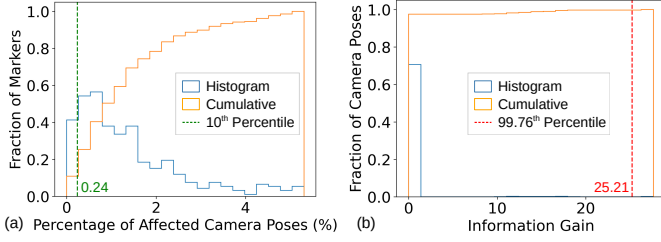


Fig. 6. Histograms for the HM3D apartment model: (a) percentage of affected camera poses and (b) information gains at camera poses yielded by a marker. The most visible 90% markers (i.e., $v = 90$) means 10th percentile in (a), determining the percentile $q = 99.76$ by (9). The 99.76th percentile in (b) indicates a localizability gain 25.21 of the marker by (6).

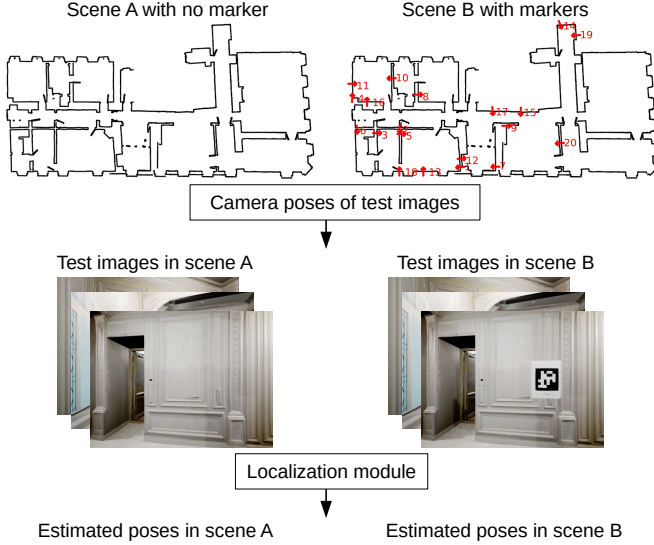


Fig. 7. The flowchart of our system for performing camera localization experiments. Scenes with different marker placements share the same set of camera poses for acquiring test images and the same localization module.

corners, to effectively join in the selection of best marker while a low v favors the most visible ones among feasible marker poses. In the ground plane space, for any marker \mathbf{m} , we can find a set of affected camera poses $\mathcal{C}_{\mathbf{m}}$ that are supposed to see the marker in the FOV (i.e., nonzero info. gain). We can derive a CDF $F_P(p)$ using percentages of affected camera poses for all markers

$$\mathcal{P} = \left\{ \frac{|\mathcal{C}_{\mathbf{m}}|}{|\mathcal{C}|} \times 100 : \mathbf{m} \in \mathcal{M} \right\}. \quad (8)$$

To ensure only the most visible v percent of markers earn nonzero localizability gains, the percentile q is determined by the $(100 - v)^{th}$ percentile in percentages of affected camera poses, as seen in

$$q = 100 - \inf \left\{ p \in [0, 100] : F_P(p) \geq \frac{100 - v}{100} \right\}. \quad (9)$$

(9) indicates q is a non-decreasing function of v . When v approaches 100, q approaches 100 as well so only markers that earn a greater maximum in information gains will be considered in the best marker selection (see (6)); when v approaches 0, q approaches 0 as well so the best marker will only be selected from markers that influence large areas.

Thus the choice of hyperparameter v can reflect the trade-off between helping the worst single camera pose and influencing the most camera poses.

Fig. 6 shows an example for computing the percentile q and the localizability gain for the marker placement in Fig. 5. We set $v = 90$ as the default setting so the most visible 90% markers receive nonzero localizability gains and are effective best marker candidates. This setting results in a marker placement strategy that tends to support worst camera poses instead of area coverage, as shown in the optimized marker placement for the apartment model in Fig. 9. No markers are placed in the two big rooms on the right of the apartment since (i) camera poses in these rooms already enjoyed good localizability scores (see Fig. 5a) and (ii) a large hyperparameter v does not emphasize area coverage.

IV. EXPERIMENTAL SETUP

A. Implementation

We implemented all three key techniques and Algorithm 1 in Sec. III-B in Python with assistance of a few open source software packages. We used the Unreal Engine 4.27 [20] and the AirSim library (v1.8.1) [21] to simulate and collect images from 3D models. We used the Open3D library [22] to downsample scan points to get candidate marker locations. We used the GTSAM library [23] to create factor graphs and estimate covariance in Gaussian approximations of camera pose distributions.

Additionally, we implemented a simulation system for testing marker placement algorithms and a camera localization module for estimating camera poses of test images. Fig. 7 presents a flowchart of the system. The system adds markers to a scene model at positions planned by marker placement algorithms and then acquires test images from the same set of camera poses for different marker placements for the fairness in comparison. We stress three advantages of the simulation system over real world pipelines for performing camera localization experiments: 1) reproducible data collection by other researchers for future development of marker placement algorithms, 2) a large number of test images that cover the scene, 3) consistent camera poses for acquiring test images in scenes with different marker placements.

B. Evaluation

1) *Methods for comparison:* We compare our algorithm OMP with 1) no marker placement and 2) random marker placements. Random marker placements refer to uniformly weighted samples from feasible marker poses. We generated 5 versions of random placements for each scene and all randomly placed markers were manually inspected in scene models to ensure reasonable quality of random placements.

2) *Scene models:* The method comparison is performed on three scene models. The models are designated with names apartment, studio, and office, as seen in Fig. 9. The first two models are pre-built dense maps of realworld spaces provided by the Habitat-Matterport 3D (HM3D) Research Dataset [15] while the last model is an Unreal Engine simulation environment that resembles typical realworld offices³. Table I lists specifics of these models.

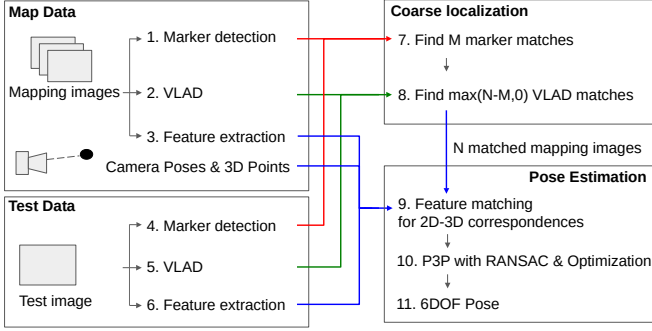


Fig. 8. The localization module using fiducial marker detection. The numbers indicate the order of different operations. The map data consists of RGB images (mapping images), camera poses, and depth for computing 3D points. The test data only includes RGB images (test images). We detect markers, compute the VLAD descriptor, and extract features for any RGB image. The markers and the VLAD descriptor of a test image are used to find N best matches in the mapping images. Feature points in the matched images are used to estimate the pose of the test image.

3) *The localization module*: Fig. 8 presents the flowchart of our localization module. The localization module is similar to standard approaches [24] but with an extra function of fiducial marker detection. The fiducial marker detection was provided by the AprilTag library [4]. Our implementation of VLAD descriptors [25] was adapted from [26]. The tag detection and VLAD descriptors were sequentially employed to find 10 matched images in the map data (i.e., $N = 10$ in Fig. 8). Camera poses were estimated using P3P [27] with RANSAC [28] followed by Levenberg-Marquardt optimization [29]. The rotation error δ_R is defined as the angular distance between the estimated rotation matrix \hat{R} and the groundtruth rotation R while the translation error δ_t is defined as the Euclidean distance between the estimated translation \hat{t} and the groundtruth translation t , as seen in

$$\delta_R = \left| \arccos\left(\frac{\text{tr}(\hat{R}^T R) - 1}{2}\right) \right|, \quad (10)$$

$$\delta_t = \|\hat{t} - t\|_2. \quad (11)$$

4) *The map and test data*: The camera poses for collecting the map data are the same as the feasible camera poses in the ground plane space. The camera poses for collecting test images are sampled from the feasible camera poses with weights and then perturbed by translation and rotation noises that are subject to a uniform distribution in $[-0.5, 0.5]$. The weights in the sampling correlate with localizability scores for generating more test images around low-scoring camera poses. Let $\mathcal{L} = \{l(\mathbf{c}) : \mathbf{c} \in \mathcal{C}\}$ be the set of localizability scores of feasible camera poses in the ground plane space with no markers. The weights are defined as

$$\mathcal{W} = \{2l^* - \bar{l} - l(\mathbf{c}) : \mathbf{c} \in \mathcal{C}\}, \quad (12)$$

where l^* is the maximal score in \mathcal{L} and \bar{l} is the mean of all scores. Thus all weights will be non-negative and a lower score incurs a greater weight.

³The serial number of the apartment model is 00770-NBg5UqG3di3 in the HM3D dataset and that of the studio model is 00254-YMNvYdhK8mB. The office model is the ThreeDee Office project in the Unreal Engine Marketplace.

TABLE I. Specifics of models

Model	Area (m^2)	# of map images	# of test images
Apartment	339.3	10856	10000
Studio	149.6	2832	3000
Office	108.3	1768	2000

V. RESULTS

We present three sections of results. In the first section, we present results comparing different marker placement methods. Next, we show a parameter study about factors that can affect our algorithm and the localization performance. Finally, we present a sensitivity study about the influence of marker position and size deviations on the localization performance. The recall is defined as the percent of localized images in all test images and is the main metric we use. A test image is recognized as being localized if the translation error is lower than 5cm and the rotation error is lower than 5 degrees. The default hyperparameter v is 90.

A. Comparison of Marker Placement Methods

Optimized marker placements for three scene models can be found in Fig. 9. It is evident that our algorithm focuses on placing markers around low-scoring areas and improves mean localizability scores by a large margin. For example, the largest room in the studio model only receives a single marker (marker 9 on the top right of the studio) since the room already possesses good localizability scores even with no markers.

Optimized marker placements consistently outperform no marker placement and random placements on the recall. Optimized marker placements and 5 sets of random marker placements were separately applied to each model for performing camera localization experiments. The recall of test images for the three models can be found in Fig. 9. After placing 20 markers, our algorithm improves the recall by over 1.5 percentages for the apartment model, 3.0 percentages for the studio model, and 20.0 percentages for the office model. Note that the area of the apartment model is very big and the model has attained a high recall 85% with no assistance of markers so the increment of recall for the apartment model was expected to be lower than that for the other models.

B. Parameter Study

In the parameter study, we design three experiment groups and change one of the default parameters in each experiment group. The experiment groups are 1) different values of v in the greedy algorithm, 2) enabling/disabling tag detection in the localization module, and 3) low-scoring/uniform test data, as seen in Table II. The default setting is with $v = 90$, tag detection enabled, and the low-scoring test data that has more test images in low-scoring areas in the ground plane. For the parameter study, we use the office model.

Too large or small values of hyperparameter v incur lower improvements of the recall. The hyperparameter was introduced to compute the localizability gain of a marker. As explained in Sec. III-B.3, lower v favors markers that cover

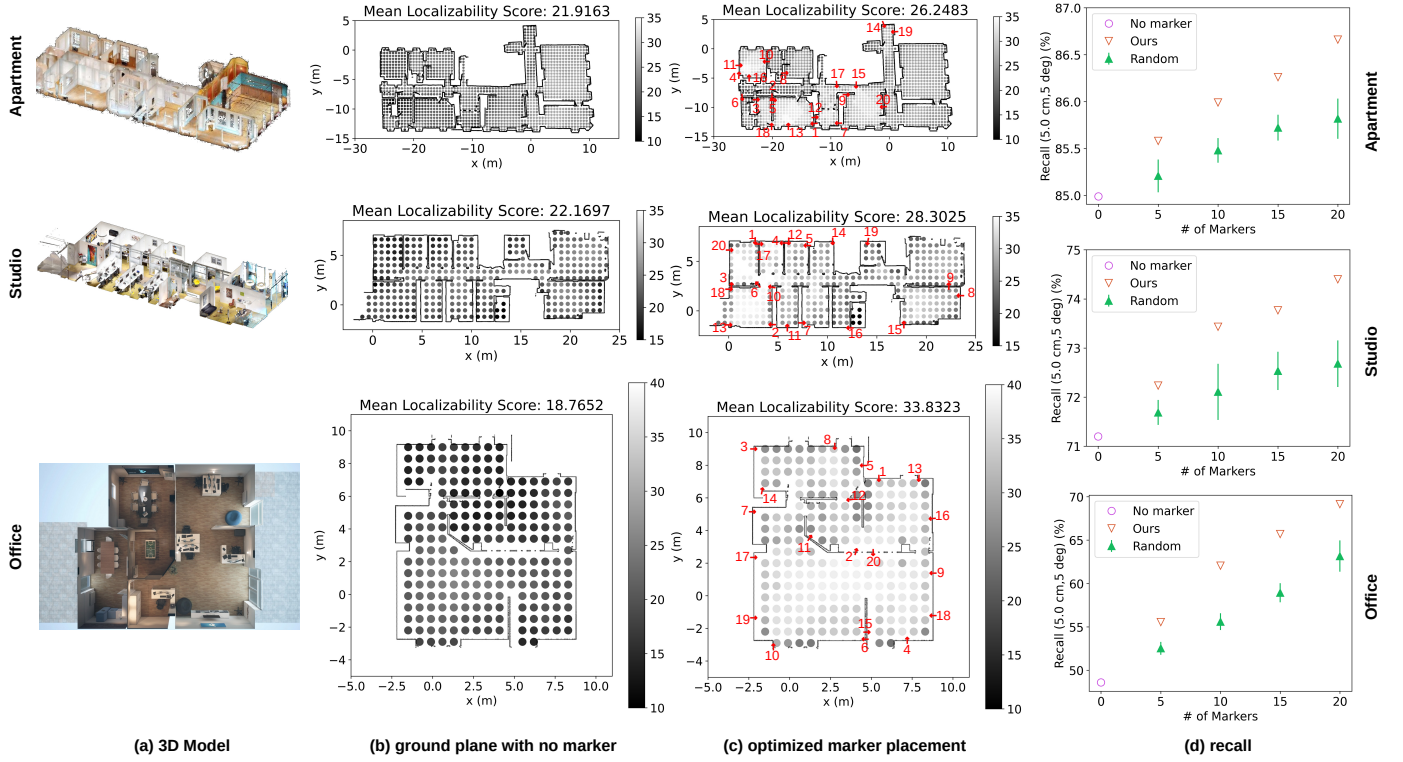


Fig. 9. Results for three scene models: (a) 3D scene models, (b) ground plane space with no markers where darker dots indicate lower localizability scores, (c) optimized marker placements where the red arrows represent optimized marker placements and the numbers beside the arrows indicate the order of marker placements, and (d) the recall in camera localization experiments where we generated 5 random placements for each scene and report the mean and standard deviation.

TABLE II. Parameter study about the hyperparameter v , the test data, and enabling/disabling tag detection. The default (df.) setting is with $v = 90$, tag detection enabled, and the low-scoring test data. The hyperparameter v means selecting best poses among the most visible $v\%$ feasible marker poses. The uniform test data means test images are uniformly sampled from the ground plane while the low-scoring data means sampling test images with weights favoring low-scoring areas. No tag ID and relative pose are retrieved when tag detection is turned off.

Experiment group	Recall of test images with k markers (%)				
	$k = 0$	5	10	15	20
$v = 90$ (df.)	48.6	55.5	62.1	65.7	69.2
$v = 99$	48.6	55.5	60.4	64.5	67.4
$v = 70$	48.6	54.8	61.1	63.2	66.6
$v = 50$	48.6	54.3	57.6	63.9	66.8
Tag detect. on (df.)	48.6	55.5	62.1	65.7	69.2
Tag detect. off	48.6	55.2	60.7	64.2	67.5
low-scoring data (df.)	48.6	55.5	62.1	65.7	69.2
Unif. test data	57.4	63.7	68.4	72.1	74.8

larger areas while greater v tends to stress the worst single camera pose. Table II shows that the default value ($v = 90$) consistently outperforms small value 50 and large value 99, indicating that the default attains a good balance between area coverage and helping the worst cases.

The localizability score can be a good indicator of localization errors. As explained in Sec. IV-B.4, we sampled more test images in low-scoring areas by the default setting. Now we are curious about the recall of test images that are uniformly sampled in the ground plane space. Table II shows

that uniform test samples enjoy greater recall than test samples that stress low-scoring areas by at least 5 percentages.

Both the texture and ID of tags are helpful for localization. We disable tag detection in the localization module (Fig. 8) to investigate the impact of tag detection on the recall. Table II shows that tags still improve the recall even though the tag detector is turned off (i.e., no tag ID and relative pose). The reason is that the texture of markers is still helpful for coarse localization and pose estimation in the localization module.

C. Sensitivity study of marker sizes and positions

It is quite likely that a user will not be able to place fiducial markers exactly at the positions computed by the OMP algorithm; meanwhile, different users may print fiducial markers with different sizes. Thus we investigate the impact of position deviations and marker sizes on the recall. For the sensitivity study, we used the office model.

Enlarging markers up to a certain size keeps increasing the recall. Fig. 10a shows that, under 50 cm, larger tag widths lead to greater recall (note that the threshold 50 cm should correlate with environments). Excessively large sizes can degrade the recall because the markers become too big to be detected from nearby views.

Mild position deviations slightly degrade the performance of the optimized marker placement. All 20 markers planned by the OMP algorithm were moved left or right by certain distances to implement position deviations. Fig. 10b shows the recall can decrease by 2% in the presence of ± 0.25 meters position deviations and by 5% in the presence of ± 1

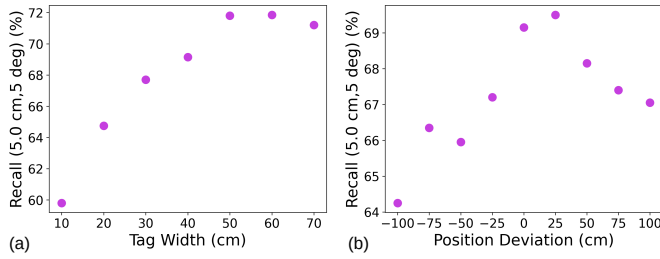


Fig. 10. Sensitivity study: (a) re-sizing tags and (b) applying different position deviations to marker poses planned by the OMP algorithm.

meter position deviations, compared with zero position deviation. However, marker placements with the position deviations still outperform no marker placement by a large margin (~ 15 percentages in the recall).

VI. CONCLUSION AND FUTURE WORK

This work provides a promising foundation for optimizing and evaluating marker placement for improved visual localization. Our OMP algorithm defines localizability scores for different areas in the scene and uses a greedy algorithm to find the best marker placements in the sense of increased localizability scores. We applied the OMP algorithm to three scenes and demonstrated that OMP consistently improves camera localization recall compared to random marker placements and no marker placement.

The OMP algorithm only considers placing markers in a scene model (i.e., mapped areas in the scene), however, hard locations that are not able to be mapped are probably the best places for markers. The algorithm can be extended with a hole-filling approach that prioritizes marker placements in unmapped areas (i.e., holes on model surfaces) if needed. Further research is also needed to compute more accurate localizability scores and explore more efficient optimization methods beyond the greedy algorithm, including: (1) joint optimization of marker poses and sizes, (2) extending the single-layer ground plane to multi-layer planes, (3) using non-Gaussian distribution estimation techniques to compute localizability scores, and (4) applying submodular optimization to jointly select multiple best markers together with fewer iterations.

REFERENCES

- [1] Z. Zhang, T. Sattler, and D. Scaramuzza, "Reference pose generation for long-term visual localization via learned features and view synthesis," *Int. J. Comput. Vis.*, vol. 129, no. 4, pp. 821–844, 2021.
- [2] R. Muñoz-Salinas and R. Medina-Carnicer, "UcoSLAM: Simultaneous localization and mapping by fusion of keypoints and squared planar markers," *Pattern Recognit.*, vol. 101, p. 107193, May 2020.
- [3] J. DeGol, T. Bretl, and D. Hoiem, "Improved structure from motion using fiducial marker matching," in *Proc. Eur. Conf. Comput. Vis.*, 2018, pp. 281–296.
- [4] E. Olson, "AprilTag: A robust and flexible visual fiducial system," in *Proc. IEEE Int. Conf. Robot. Autom.*, 2011, pp. 3400–3407.
- [5] S. Garrido-Jurado, R. Muñoz-Salinas, F. Madrid-Cuevas, and M. Marín-Jiménez, "Automatic generation and detection of highly reliable fiducial markers under occlusion," *Pattern Recognit.*, vol. 47, no. 6, pp. 2280–2292, 2014.
- [6] J. DeGol, T. Bretl, and D. Hoiem, "Chromatag: A colored marker and fast detection algorithm," in *Proc. IEEE Int. Conf. Comput. Vis.*, 2017, pp. 1481–1490.

- [7] Z. Zhang, Y. Hu, G. Yu, and J. Dai, "DeepTag: A general framework for fiducial marker design and detection," *IEEE Trans. Pattern Anal. Mach. Intell.*, 2022.
- [8] R. Mur-Artal and J. D. Tardós, "ORB-SLAM2: An open-source SLAM system for monocular, stereo, and RGB-D cameras," *IEEE Trans. Robot.*, vol. 33, no. 5, pp. 1255–1262, Oct. 2017.
- [9] X. Gao, R. Wang, N. Demmel, and D. Cremers, "LDSO: Direct sparse odometry with loop closure," in *Proc. IEEE/RSJ Int. Conf. Intell. Robots Syst.*, 2018, pp. 2198–2204.
- [10] Y. Chen, J.-A. Francisco, W. Trappe, and R. P. Martin, "A practical approach to landmark deployment for indoor localization," in *Proc. IEEE Commun. Soc. Sens. Ad Hoc Commun. Netw.*, vol. 1, 2006, pp. 365–373.
- [11] M. P. Vitus and C. J. Tomlin, "Sensor placement for improved robotic navigation," *Proc. Robot.: Sci. Syst.*, pp. 217–224, 2011.
- [12] D. B. Jourdan and N. Roy, "Optimal sensor placement for agent localization," *ACM Trans. Sens. Netw.*, vol. 4, no. 3, pp. 1–40, May 2008.
- [13] M. Beinhof, J. Müller, and W. Burgard, "Effective landmark placement for accurate and reliable mobile robot navigation," *Robot. Auton. Syst.*, vol. 61, no. 10, pp. 1060–1069, Oct. 2013.
- [14] Z. Lei, X. Chen, Y. Tan, X. Chen, and L. Chai, "Optimization of directional landmark deployment for visual observer on SE(3)," *IEEE Trans. Ind. Electron.*, pp. 1–10, 2022.
- [15] S. K. Ramakrishnan *et al.*, "Habitat-matterport 3d dataset (HM3D): 1000 large-scale 3d environments for embodied AI," in *Proc. Conf. Neural Inform. Process. Syst. Dataset. Benchmark. Track (Round 2)*, 2021.
- [16] D. G. Lowe, "Distinctive image features from scale-invariant keypoints," *Int. J. Comput. Vis.*, vol. 60, no. 2, pp. 91–110, Nov. 2004.
- [17] C. Stachniss, G. Grisetti, and W. Burgard, "Information gain-based exploration using rao-blackwellized particle filters," in *Proc. Robot.: Sci. Syst.*, vol. 2, 2005, pp. 65–72.
- [18] C. M. Bishop, *Pattern recognition and machine learning*. New York, USA: Springer, 2006.
- [19] M. Kaess and F. Dellaert, "Covariance recovery from a square root information matrix for data association," *Robot. Auton. Syst.*, vol. 57, no. 12, pp. 1198–1210, Dec. 2009.
- [20] Epic Games, "Unreal engine." [Online]. Available: <https://www.unrealengine.com>
- [21] S. Shah, D. Dey, C. Lovett, and A. Kapoor, "Airsim: High-fidelity visual and physical simulation for autonomous vehicles," in *Proc. Field Serv. Robot.* Springer, 2018, pp. 621–635.
- [22] Q.-Y. Zhou, J. Park, and V. Koltun, "Open3D: A modern library for 3D data processing," *arXiv:1801.09847*, 2018.
- [23] F. Dellaert *et al.*, "borglab/gtsam," May 2022. [Online]. Available: <https://doi.org/10.5281/zenodo.5794541>
- [24] P.-E. Sarlin, C. Cadena, R. Siegwart, and M. Dymczyk, "From coarse to fine: Robust hierarchical localization at large scale," in *Proc. IEEE/CVF Conf. Comput. Vis. Pattern Recognit.*, 2019, pp. 12 716–12 725.
- [25] H. Jégou, F. Perronnin, M. Douze, J. Sánchez, P. Pérez, and C. Schmid, "Aggregating local image descriptors into compact codes," *IEEE Trans. Pattern Anal. Mach. Intell.*, vol. 34, no. 9, pp. 1704–1716, Sep. 2012.
- [26] J. Guevara, "Python implementation of VLAD descriptors," <https://github.com/jorjasso/VLAD>, 2022.
- [27] X.-S. Gao, X.-R. Hou, J. Tang, and H.-F. Cheng, "Complete solution classification for the perspective-three-point problem," *IEEE Trans. Pattern Anal. Mach. Intell.*, vol. 25, no. 8, pp. 930–943, Aug. 2003.
- [28] M. A. Fischler and R. C. Bolles, "Random sample consensus: a paradigm for model fitting with applications to image analysis and automated cartography," *Commun. ACM*, vol. 24, no. 6, pp. 381–395, 1981.
- [29] G. Bradski, "The OpenCV Library," *Dr. Dobbs's Journal of Software Tools*, 2000.